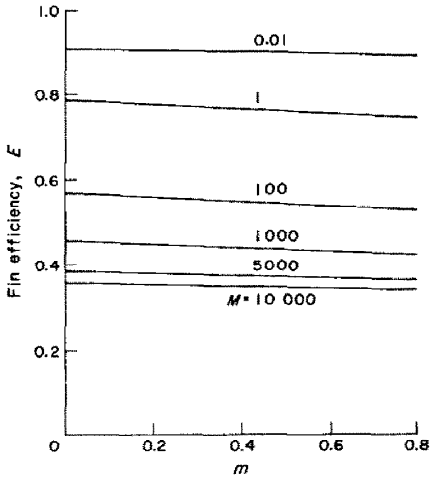


FIG. 6. Variation of fin efficiency with the fin profile geometry, $m$, for different fin parameters, $M$.

$m$ gives rise to higher local heat transfer coefficients at the tip, whereas at the base, the heat transfer coefficients are asymptotically converging to a finite value. Similarly for a given shape of the profile of the fin chosen, an increase in the magnitude of the fin parameter, $M$, has resulted in a substantial increase in heat transfer coefficients. Equation (15) is shown plotted in Fig. 5 to depict the variation of the average Nusselt number for different configurations and fin parameters. It is obvious from the results that a reduction of the material of the fin would lead to thinner films resulting in higher values for the average heat transfer coefficients. Equation (16) reveals the efficiency of the fin. The results in Fig. 6 reveal that for chosen values of $m$, the efficiency seems to be strongly dependent on the fin parameter, $M$, and $m$ has no perceptible influence for low values of $M$. However, in terms of the augmentation ratio defined as $(h/h_{so})$ for any given location, the fin gives substantially higher heat transfer coefficients and the ratio is more than one. This aspect would be of utmost significance which affects the compactness of heat pipes employing fins either inside or outside of the heat pipe. In conclusion, this note gives salient results for a wide range of parameters related to the condensation phenomena on vertical extended surfaces of varying thickness, hitherto not solved.

*Acknowledgement*—The authors would like to thank the University Grants Commission, New Delhi, for the financial support under Departmental Research Support Programme, Department of Mechanical Engineering.

## REFERENCES

1. H. Merte, Jr., Condensation heat transfer. In *Advances in Heat Transfer*, Vol. 9. Academic Press, New York (1973).
2. S. V. Patankar and E. M. Sparrow, Condensation on an extended surface, *Trans. ASME J. Heat Transfer* **101**, 434–440 (1979).
3. J. E. Wilkins, Jr., A discussion on condensation on an extended surface, *Trans. ASME J. Heat Transfer* **102**, 186–187 (1980).
4. J. H. Lienhard and V. K. Dhir, Laminar film condensation on non-isothermal and arbitrary heat flux surfaces and on fins, *Trans. ASME J. Heat Transfer* **96**, 197–203 (1974).
5. D. Poulikakos and A. Bejan, Fin geometry for minimum entropy generation in forced convection, *Trans ASME J. Heat Transfer* **104**, 616–623 (1982).
6. E. M. Sparrow and J. L. Gregg, A boundary layer treatment of laminar film condensation, *Trans. ASME J. Heat Transfer* **81**, 13–18 (1959).

*Int. J. Heat Mass Transfer.* Vol. 31, No. 9, pp. 1944–1947, 1988
Printed in Great Britain

0017-9310/88 $3.00 + 0.00


# Effect of waves on Nusselt condensation

MAZHAR ÜNSAL†
Department of Mechanical Engineering, University of Hawaii at Manoa, Honolulu, Hawaii, U.S.A.

(*Received* 1 *May* 1987 *and in final form* 14 *March* 1988)

## INTRODUCTION

NUMEROUS analyses of steady laminar condensate films flowing under the action of gravity down a vertical isothermal plane surface and adjacent to a saturated quiescent vapour have appeared in the heat transfer literature. Analyses presented by Nusselt [1], Rohsenow [2], and Sparrow and Gregg [3] are examples of earlier original work on the subject.

Previous analyses of film condensation available in the literature have not focused attention on the effect of surface waves on the heat transfer through a condensate film and this subject is considered in the present study. The transient temperature field in a condensate film oscillating with an amplitude equal to the equilibrium wave amplitude predicted by the non-linear stability theory is utilized to compute a transient heat transfer coefficient. The transient heat transfer coefficient is then averaged with respect to time and space. The predicted average heat transfer coefficient is compared with the experimental data of Ritani and Shekriladze [4].

## DISCUSSION

Previous results from the linear stability analysis of laminar film condensation [5] have shown that a laminar condensate film adjacent to a quiescent vapour is stable up to a critical distance from the leading edge of an isothermal vertical plate and unstable thereafter. The non-linear stability analysis in ref. [6] has shown that the linearly stable part of the film is also stable with respect to finite amplitude disturbances. The linearly unstable part of the condensate film, on the other hand, was found to reach finite equilibrium amplitudes provided that the Reynolds number is small and within the validity region of the long-wave perturbation analysis.

The analysis of the problem is outlined in the Appendix. Equations (4)–(6), (10) and (11) are simplified expressions valid for small $F$. It is noted that these formulas will apply to a wide range of situations since $F$ is usually small in most practical applications. To the best knowledge of the author, an experimental study on the stability characteristics of condensate films is not available in the literature. Equations (4)–(6) are also valid for isothermal liquid films and comparison of the most unstable wave number and equilibrium amplitude with experiments are presented in Figs. 1–4 for the experimental data of Kapitza [7].

† On leave from the Department of Mechanical Engineering, University of Gaziantep, 27310 Gaziantep, Turkey.

## NOMENCLATURE

| | |
|---|---|
| $a$ | wave amplitude |
| $c_{i1}$, $c_{i3}$ | linear and non-linear wave amplification rates |
| $F$ | acceleration effect parameter, $k\Delta T/(\rho v h_{fg})$ |
| $g$ | gravitational acceleration |
| $h$ | heat transfer coefficient |
| $h_{fg}$ | enthalpy of phase change |
| $H$ | dimensionless heat transfer coefficient, $(h/k)(v^2/g)^{1/3}$ |
| $\bar{H}$ | time averaged dimensionless heat transfer coefficient, $\lim_{\tau\to\infty}(1/\tau)\int_0^\tau H\,d\tilde{\tau}$ |
| $\bar{\bar{H}}$ | time and space averaged heat transfer coefficient, $(1/\tilde{L})\int_0^{\tilde{L}}\bar{H}\,dx$ |
| $k$ | liquid thermal conductivity |
| $\tilde{L}$ | length of plate |
| $L$ | dimensionless plate length, $\tilde{L}/(2v^2/g)^{1/3}$ |
| $N$ | dimensionless surface tension parameter, $2^{1/3}\sigma/\rho v^{4/3}g^{1/3}$ |
| $R$ | local Reynolds number, $g\tilde{\eta}_0^3/2v^2$ |
| $R_c$ | critical value of $R$, $[(15/4)(NF/3)^{1/2}]^{6/11}$ |
| $Re$ | local Reynolds number based on average velocity |
| $\overline{Re}$ | time averaged local Reynolds number |
| $\overline{Re}_L$ | value of $\overline{Re}$ at lower end of plate |
| $\tilde{t}$ | time |
| $\tilde{T}, \tilde{T}_s, \tilde{T}_w$ | liquid, saturation, wall temperature |
| $\Delta T$ | $\tilde{T}_s - \tilde{T}_w$ |
| $(\tilde{x}, \tilde{y})$ | axial and transverse physical coordinates |
| $y$ | dimensionless transverse coordinate, $\tilde{y}/\tilde{\eta}_0$ |
| $\tilde{x}_c$ | critical distance |
| $X$ | $\tilde{x}/\tilde{L}$ |
| $X_c$ | $\tilde{x}_c/\tilde{L} = R_c^{4/3}/2FL$. |

Greek symbols

| | |
|---|---|
| $\alpha$ | wave number, $2\pi\tilde{\eta}_0/\lambda$ |
| $\tilde{\eta}_0$ | local film thickness |
| $\theta$ | dimensionless liquid temperature, $\theta_0+\alpha\theta_1+O(\alpha^2)$ |
| $\bar{\theta}$ | time averaged dimensionless liquid temperature |
| $\lambda$ | wavelength |
| $v$ | liquid kinematic viscosity |
| $\rho$ | liquid density |
| $\sigma$ | surface tension |
| $\psi$ | dimensionless liquid stream function. |

Subscript

| | |
|---|---|
| $y$ | partial differentiation with respect to $y$. |

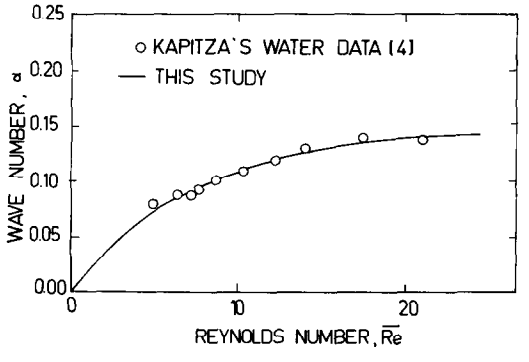


FIG. 1. Comparison of Kapitza's water data on wave number with theory.

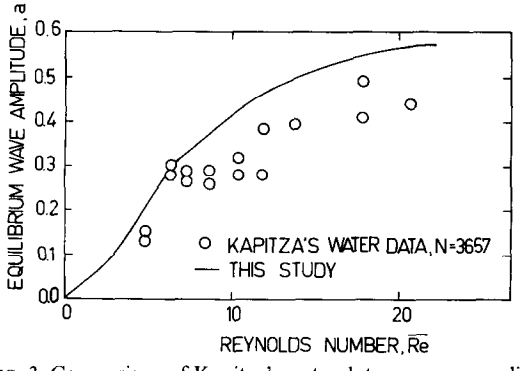


FIG. 3. Comparison of Kapitza's water data on wave amplitude with theory.

The time averaged value of the liquid film thickness is larger for a liquid film with finite amplitude waves than that given by analyses based on the steady flow assumption. The Reynolds number, $\overline{Re}$, given by equation (8) and the time averaged value of the dimensionless temperature gradient given by equation (2) depend on the wave amplitude. The following procedure was followed when plotting theoretical curves presented in Figs. 1–4. An arbitrary value of $R$ is used to compute $\alpha$ from equation (5). This computed $\alpha$ and $R$ are substituted into equation (6) to estimate the wave amplitude. Next, $b_r$ and $b_i$ are computed from equations (10) and (11). The wave amplitude together with $b_r$ and $b_i$ are used in equation (8) to estimate the liquid Reynolds number. It is noted that the simpler relationship $\overline{Re} = 2R/3$ is valid for

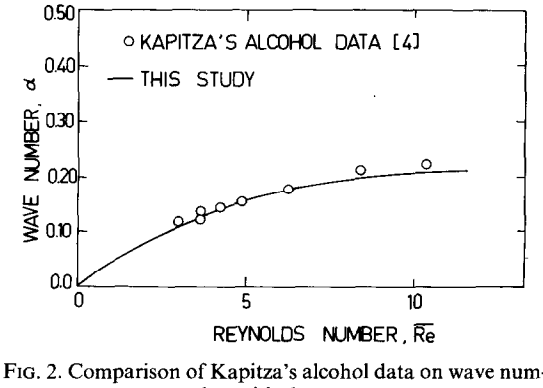


FIG. 2. Comparison of Kapitza's alcohol data on wave number with theory.

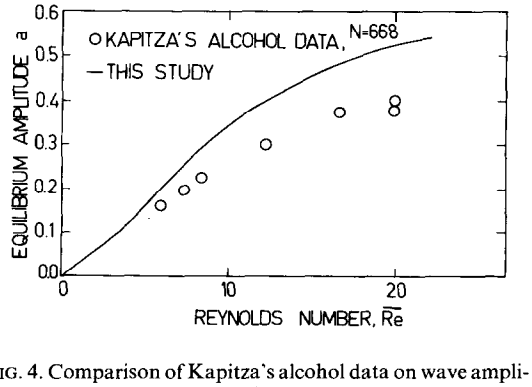


FIG. 4. Comparison of Kapitza's alcohol data on wave amplitude with theory.

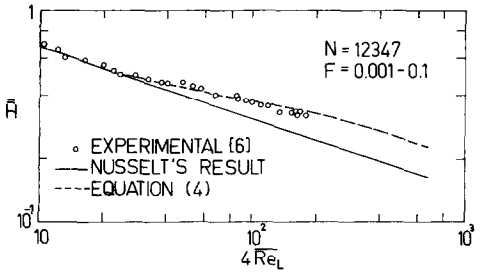


FIG. 5. Comparison of experimental dimensionless average heat transfer coefficient with theory.

waves of infinitesimal amplitude only and that equation (8) must be used for liquid films with finite amplitude waves.

The dashed curve in Fig. 5 shows the time and space averaged dimensionless heat transfer coefficient estimated from equation (14). Also shown in this figure are experimental data from ref. [4]. The solid curve in this figure represents the theoretical result corresponding to a Nusselt type analysis given by equation (13).

The author repeated the evaluation of equation (14) using the general form of the expressions for the most probable wave number, the equilibrium wave amplitude, and expressions for $b_r$ and $b_i$ given in ref. [6] rather than using the simplified expressions (5), (6), (10) and (11) given in this study. The same theoretical dashed curve shown in Fig. 5 was obtained. The computation of $\bar{H}$ was further repeated for values of the acceleration effect parameter, $F$, ranging from 0.001 to 0.1 and values of the surface tension parameter, $N$, ranging from 100 to 10 000. It was found that changing $F$ from 0.001 to 0.1 has less than a 1% effect on the value of $\bar{H}$ when $\overline{Re_L} < 250$. Decreasing $N$ from 10 000 to 100 resulted in an increase of $\bar{H}$ from 0.1177 to 0.1207 (only a 2.5% change) when $\overline{Re_L} = 248$. The percentage change in $\bar{H}$ was lower at smaller values of $\overline{Re_L}$. It is therefore concluded that surface tension has a small effect on the heat transfer from a wavy condensate film when $N < 10\,000$. If the surface tension parameter is increased to values larger than 10 000, the critical value of $R$, $R_c$, and the critical distance $X_c$ both increase. The theoretical dashed curve depicted in Fig. 5 then comes closer to the solid line.

## CONCLUSION

It is seen that predictions from stability analyses for the wave number and the equilibrium wave amplitude are in fair agreement with the experimental data of Kapitza. Prediction of the dimensionless average heat transfer coefficient, $\bar{H}$, based on the transient temperature field determined from stability analyses is in good agreement with experimental data which is a strong indication that the deviation of experimental data of ref. [4] from the Nusselt solution is a result of waves on the condensate film.

## REFERENCES

1. M. Jacob, *Heat Transfer*, p. 663. Wiley, New York (1967).
2. W. M. Rohsenow, Heat transfer and temperature distribution in laminar-film condensation, *Trans. ASME* **78,** 1645–1648 (1956).
3. E. M. Sparrow and J. L. Gregg, A boundary layer treatment of laminar film condensation, *J. Heat Transfer* **81,** 13–18 (1959).
4. S. V. Ritani and T. G. Shekriladze, An experimental study of the heat exchange process on transition from laminar to turbulent flow of the film, *Thermal Engng* **II,** 101–102 (1964).
5. M. Ünsal and W. C. Thomas, Linearized stability analysis of film condensation, *J. Heat Transfer* **100,** 629–634 (1978).
6. M. Ünsal and W. C. Thomas, Nonlinear stability of film condensation, *J. Heat Transfer* **102,** 483–488 (1980).
7. D. ter Haar (Editor), *Collected Papers of P. L. Kapitza*, pp. 662–709. Pergamon Press, Oxford (1965).
8. Errata, *J. Heat Transfer* **105,** 216 (1983).

## APPENDIX

The transient temperature is directly adapted from the closed form solution given in ref. [6]. The dimensionless transient temperature in the film given in equation (13) of ref. [6] is used to evaluate the following space and time averaged dimensionless heat transfer coefficient. The nomenclature used is the same as that in ref. [6]

$$\bar{H} = \int_0^1 (\bar{\theta}_{0r}/(2R)^{1/3})\,\mathrm{d}X + O(\alpha^2) \tag{1}$$

where $\bar{\theta}_{0r}$ is obtained from equations (14) and (17) of ref. [6] as

$$\bar{\theta}_{0r} = 1 + a^2/2 + (b_r^2 + b_i^2 - 3b_r + 3)a^4/8 + O(a^6) + O(\alpha^2) \tag{2}$$

where

$$a^2 = -c_{11}/c_{13}. \tag{3}$$

The wave amplitude given by equation (3) is a function of the wave number. It is therefore necessary to select a proper wave number in order to predict a wave amplitude. The natural choice is the wave number having the largest amplification rate. The following simplified form of the linear wave amplification rate will be used (from equation (34) of ref. [6] with $k_0 = 0$, $k_1 = \alpha$, $k_2 = \alpha/2$)

$$\alpha c_{i1} = (8\alpha^2 R/15 - \alpha^4 N R^{-2/3}/3)/(1 + 25\alpha^2 R^2/144). \tag{4}$$

The wave number which maximizes this expression is given by

$$\alpha = [-144/25R^2 + ((144/25R^2)^2 + 3456/375NR^{1/3})^{1/2}]^{1/2}. \tag{5}$$

Equation (43) of ref. [6] will be utilized to compute the equilibrium amplitude. An algebraic error was previously noted in that equation [8]. To correct this error, the integer 131 in equation (43) of ref. [6] will be replaced by the integer 47. The corrected form of the equation is as follows:

$$a^2 = (8/15 - \alpha^2 N/3R^{5/3})NR^{1/3}\alpha^4/(1 + 47NR^{1/3}\alpha^4/80 + 57\alpha^2 R^2/400 - \alpha^6 N^2/72R^{4/3}). \tag{6}$$

The film Reynolds number defined as the ratio of mass flow rate (per unit width) to dynamic viscosity is expressed as

$$Re = R\psi. \tag{7}$$

The time average of equation (7) yields

$$\overline{Re}/R = \tfrac{2}{3} + a^2 + (b_r^2 + b_i^2 + b_r)a^4/4 + O(a^6) + O(\alpha^2). \tag{8}$$

Variation of $R$ with axial dimensionless distance $X$ will be determined from equation (18) of ref. [6]. This equation, after simplification for $F = 0$, neglecting terms of order $\alpha^2$ and using equation (27) of ref. [6] for $S_2$, becomes

$$\frac{\mathrm{d}R}{\mathrm{d}X} = \tfrac{3}{2}FL(1 + a^2/2)R^{-1/3} + O(\alpha^2). \tag{9}$$

Real and imaginary components of $b$ for small $F$ are expressed by

$$b_r = 1/6 - 3R^{5/3}/10N\alpha^2 \tag{10}$$

$$b_i = -R^{2/3}/N\alpha^3. \tag{11}$$

If all of the condensate film of length $\tilde{L}$ is stable then equation (8) will read

$$\overline{Re}/R = 2/3 \quad \text{with} \quad R = (2FLX)^{3/4}. \tag{12}$$

For a stable film, equation (1) can be expressed as

$$\bar{H} = 4/3^{4/3}\overline{Re}_1^{1/3}. \tag{13}$$

For a film with a wavy section ($X_c < 1$) equation (1) becomes

$$\bar{\bar{H}} = 2^{2/3} R_c/3FL + \int_{X_c}^{1} (\bar{\theta}_{0y}/(2R)^{1/3})\,dX \qquad (14)$$

where $\bar{\bar{H}}$ may be estimated provided that values of $F$, $N$ and $L$ are specified. The integral in equation (14) was estimated by determining $X_c$ and $R_c$, evaluating the wave number from equation (5), estimating wave amplitude and $b$ from equations (6), (10) and (11), numerically integrating equation (9) for $X > X_c$, and using equation (2) in equation (14).

*Int. J. Heat Mass Transfer.* Vol. 31, No. 9, pp. 1947–1952, 1988
Printed in Great Britain

0017–9310/88 $3.00 + 0.00


# Dynamic instability experiments in a boiling flow system

R. P. Roy and P. Jain

Department of Mechanical and Aerospace Engineering, Arizona State University, Tempe, AZ 85287, U.S.A.

and

S. P. Kalra

Electric Power Research Institute, Palo Alto, CA 94303, U.S.A.

(*Received* 19 *September* 1987 *and in final form* 8 *March* 1988)

## INTRODUCTION

Thermally driven flow instabilities in vapor (gas)–liquid flow systems can give rise to major operational problems in various equipment and components of importance. Severe mechanical vibrations and thermal stresses may result from these instabilities. Onset of critical heat flux may also be hastened, leading to burnout of the heated section.

Experimental studies of dynamic instabilities aimed at identifying the instability threshold condition in vapor–liquid flow systems have been numerous (e.g. refs. [1–6]). These studies indicate that the most common dynamic instability is a low frequency (0.1–2 Hz, typically) flow oscillation of the limit cycle type termed density wave oscillations (DWO). Brimley *et al.* [4] made an interesting observation that the onset of instability was frequently not an abrupt phenomenon. Rather, the amplitude of flow oscillations (the test section inlet flow rate was usually the measured variable) increased gradually with increase in heat input. On the other hand, experiments such as ref. [5] reported reasonably clear boundaries across which the flow oscillation amplitude increased sharply.

Our experimental study of a Refrigerant-113 boiling flow system was undertaken as one part of a research effort the goals of which encompassed both theoretical modeling and experiments. The main objective of the experiments was to generate our own data base for validating a dynamic instability model developed in the course of the theoretical effort. One other set of experimental data had been reported earlier for a Refrigerant-113 system [5]. The main difference between our data and those of ref. [5] lies in the geometric configuration of the test section, this being annular with a rather large flow area in our case and tubular in ref. [5].

Our other objective was to visually inspect the subcooled boiling flow field during the inception of flow instability with particular emphasis on the region where significant net vapor generation began. The annular test section with a transparent outer section (pipe) allowed flow visualization as well as flash photography.

## EXPERIMENTAL APPARATUS

A schematic diagram of the experimental rig is shown in Fig. 1. The annular test section was oriented vertically, the flow of fluid being upward through it. The outer section of the annulus was comprised of two long segments of transparent pyrex glass pipe (38.1 mm i.d., 47.0 mm o.d.). A 304 stainless steel tube of 15.9 mm o.d. and 1.2 mm wall thickness constituted the inner section of the annulus. The overall test section was 3.66 m long of which heat could be supplied to the upper 2.74 m by resistively heating the inner tube by direct current (the maximum power input possible is 37 kW at present).

Two locations are marked on Fig. 1, namely junctions 1 and 2. These indicate the beginning and the end of our 'test channel', respectively. The annular test section is one part of this test channel, the others being the inlet and exit piping and components. The inlet part contains, in addition to the piping, a preheater (1 kW maximum input power), a turbine flow meter (Flow Technology) and a globe valve which provides a variable inlet flow restriction. The preheater was not operated in these instability experiments since it was important that the entire energy input to the test channel fluid be provided in the test section itself. The exit part contains a ball valve in addition to the piping. This valve provides a variable flow restriction at the test section exit. A differential pressure transducer (Tavis) was used to measure, sequentially, the pressure drops across (i) the inlet piping and components and (ii) the exit ball valve and piping.

A 316 stainless steel centrifugal pump (Ingersol Rand) circulated the fluid through the rig. The pump was capable of providing a flow rate of 570 l $min^{-1}$ (approximately 150 U.S. gpm) at 450 kPa (approximately 65 psi) total dynamic head. Typically, more than 95% of the total pump flow was diverted through a large bypass line (51 mm nominal diameter) installed parallel to the test section.

The following uncertainties apply to the primary measurements made in the course of the instability experiments:

input heating power: $\pm 10$ W
flow rate at test section inlet: $\pm 1 \times 10^{-6}$ $m^3$ $s^{-1}$
temperature at test section inlet: $\pm 0.1$ K
system pressure: $\pm 0.7$ kPa.

A dedicated system (DATA 6000, Analogic–Data Precision) equipped with a floppy disk drive and a plotter (Hewlett–Packard) was used to acquire, store and analyze the time series data obtained from the turbine flow meter–monitor.

## EXPERIMENTAL PROCEDURE

The variables that nominally described an instability test were: (i) the mean flow rate through the test section, (ii) system pressure and inlet temperature, (iii) inlet and exit flow